Journal of Nuclear Materials 392 (2009) 439–446

Contents lists available at ScienceDirect

Journal of Nuclear Materials

journal homepage: www.elsevier.com/locate/jnucmat

The effects of irradiation condition and microstructural change on lattice parameter, crystal lattice strain and crystallite size in high burnup UO_2 pellet

Masaki Amaya *, Jinichi Nakamura, Toyoshi Fuketa

Fuel Safety Research Group, Nuclear Safety Research Center, Japan Atomic Energy Agency, 2-4, Shirane Shirakata, Tokai-mura, Naka-gun, Ibaraki 319-1195, Japan

ARTICLE INFO

Article history:
Received 17 November 2008
Accepted 3 April 2009

ABSTRACT

Pellet samples (average burnup: 37–62 GWd/t) were prepared from three kinds of fuel rods which were irradiated in the Halden Heavy Water Reactor in Norway, and microstructural changes in the pellet samples were investigated by means of optical microscopy, SEM/EPMA and micro-X-ray diffractometry. The measured lattice parameters tended to be smaller than the values reported previously, and it is likely that the measured lattice parameters were affected by the temperature conditions during the irradiation tests and the microstructural changes which occurred in the samples. Considering the burnup dependence of uniform and non-uniform strains, the following things are suggested: the interstitial atoms which cause uniform strain begin firstly to form dislocations as a recovery process of irradiation defect and the dislocation density increases. With increasing burnup, the accumulation of dislocations in the crystallite saturates and the migration of dislocations becomes dominant as a recovery process of irradiation defects in the crystallite.

1. Introduction

The microstructural changes which are called "rim structure" are often observed at the periphery of high burnup LWR fuel pellets. It is well-known that rim structure is characterized by a local porosity increase and the formation of coarsened bubbles surrounded by small sub-divided grains. Since the rim structure has these special features, it is considered that the area where the rim structure is formed becomes a possible source of fission gas release in high burnup fuel pellets during normal operation or transient conditions. From the view point of fuel safety at high burnup, it is important and necessary to clarify the characteristics and formation mechanisms of the rim structure.

The accumulation of irradiation-induced defects and fission gas during irradiation is one of the probable causes of rim structure formation. Irradiation-induced defects and dissolved fission gas tend to expand the crystal lattice of UO_2 and as a consequence, lattice parameter increases are observed in irradiated UO_2. Several groups have reported the lattice parameter in irradiated UO_2 [1–3] by using X-ray diffractometry and observed lattice parameter increases with increasing burnup up to approximately 70 GWd/t. which may be the threshold burnup for rim structure formation. Recently, the authors [4] reported lattice parameters, non-uniform strains and crystallite size in LWR fuel pellets in the burnup region from 40 to about 70 GWd/t by means of X-ray diffractometry. They measured the peak broadenings of the X-rays diffracted from the irradiated fuel pellets, and discussed the strain energy density changes which were evaluated from the uniform and non-uniform strains in the crystallite in connection with the accumulation of dislocations and found a relationship between them. Although it seems that the change in the strain energy density is related to the rim structure formation, few data which can be used for strain energy evaluation have been reported excluding their study. Therefore, more data are needed to discuss the rim structure formation mechanism.

In this study, the X-ray diffractometry of the UO_2 pellets irradiated in various conditions in a test reactor is carried out in order to investigate the changes in crystallite size and non-uniform strain with the irradiation conditions. The microstructural changes which occur in the irradiated UO_2 pellets are also discussed based on the burnup dependence of crystallite size and non-uniform strain.

2. Experimental

2.1. Sample preparation

Pellet samples were prepared from three UO_2 test fuel rods irradiated in the Halden Heavy Water Reactor (HBWR) in Norway. The test rods were installed in irradiation rigs which are called "Instrumented Fuel Assemblies (IFAs)" and irradiated. Fig. 1 presents the average linear heat rate histories of the three fuel rods irradiated in the HBWR. Rod 1 was irradiated under high linear heat rate conditions (about 500 W/cm) at the beginning of irradiation and the linear heat rate gradually decreased toward the end of irradiation. As for rods 2 and 3, the irradiation under high power conditions

* Corresponding author. Tel.: +81 29 282 6386; fax: +81 29 282 5429.
E-mail address: amaya.masaki@jaea.go.jp (M. Amaya).

0022-3115/$ - see front matter © 2009 Elsevier B.V. All rights reserved.
doi:10.1016/j.jnucmat.2009.04.005

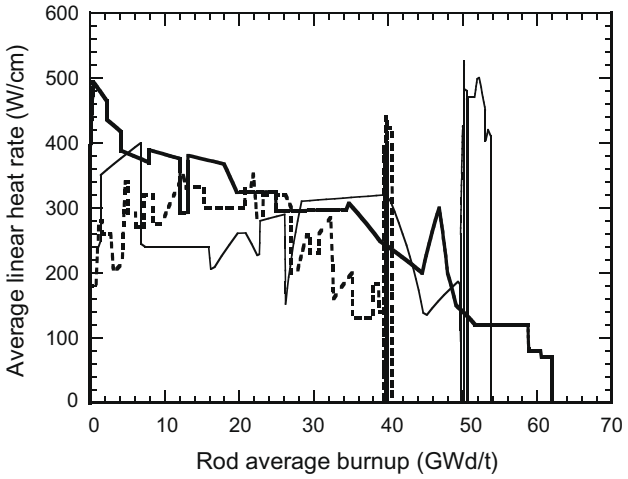

Fig. 1. Rod average linear heat rate histories of the UO_2 test rods irradiated in the HBWR. ——: rod 1, - - - -: rod 2, — : rod 3.

(about 450–500 W/cm) were carried out near the end of irradiation. The linear heat rates of rods 2 and 3 were 200–300 W/cm before the high power irradiation tests. The rod average burnups at the end of the irradiation tests were approximately 62, 41 and 54 GWd/t for rods 1, 2 and 3, respectively.

Pellet samples about 10 mm in length were cut from the test fuel rods with cladding and embedded in epoxy resin. Here, samples 1, 2 and 3 were obtained from rods 1, 2 and 3, respectively. The cross section of each sample was ground and finally polished into a specular surface using 1 μm diamond paste. In order to evaluate the accuracy of X-ray diffractometry, an unirradiated UO_2 pellet sample was also prepared using the same method.

Considering the power peaking history along the axial direction of each test rod during irradiation, the average burnups of samples 1, 2 and 3 were estimated as approximately 62, 37 and 51 GWd/t, respectively. Sample characteristics are summarized in Table 1.

2.2. Optical and scanning electron microscopy (SEM) and electron probe micro analysis (EPMA)

The sample microstructures were examined by optical and scanning electron microscopy. The microstructures on the as-polished and etched surfaces were observed. Fractured surfaces were also prepared and examined by SEM whether or not the rim structure formed in the samples.

In order to investigate the radial burnup profiles in the samples, the fission product of Nd which was retained in the fuel pellets was analyzed by electron probe micro-analysis with an electron beam diameter of 1μm. The element Nd is often used as a burnup index, because Nd is one of the elements that is soluble in the UO_2 matrix and hardly moves during irradiation. The relative concentration of Nd was obtained by dividing the characteristic X-ray intensity of Nd by that of uranium at the same location in order to eliminate any effects due to irregularities such as pores and cracks on the specimen surface.

2.3. Measurement of lattice parameter and crystallite size

2.3.1. X-ray diffractometry

X-ray diffraction measurements on irradiated UO_2 pellets were carried out by using a micro-X-ray diffractometer (RAD-3X type, Rigaku Corp.) with Ni-filtered Cu Kα radiation. The measurement part of the apparatus is set in a hot cell and can be controlled from outside of the cell. The sample was placed on the X–Y stage of the measurement part and the position of the X-ray radiation was monitored by a TV camera. The accelerating voltage and current were 40 kV and 40 mA, respectively. The diameter of the X-ray radiation area on the sample was about 0.5 mm. The diffraction angle of the goniometer was calibrated from the measurement results of a Si standard powder sample. The accuracy of the diffraction angle was better than ±0.006° in 2θ above 75°. Fig. 2 shows the radial positions of the X-ray diffraction measurement on the cross-sectional surface of each sample.

2.3.2. Measurement of lattice parameter, non-uniform strain and crystallite size

The lattice parameter and diffraction peak broadening (the increase of the full width at half maximum (FWHM) of diffraction peak) of the irradiated UO_2 pellets were evaluated from the results of X-ray diffractometry. The lattice parameter was obtained by least-squares calculations using seven diffraction lines between 75° and 130° in 2θ based on Cohen's method. The scanning speed of the goniometer was 0.25° min^{-1}. The error in the obtained lattice parameter was less than ±0.4 pm, excluding the measurement results in the vicinity of the central hole: the number of peaks obtained there was fewer due to the preferred crystal orientation which may follow the columnar grain formation near the central hole.

Since the obtained diffraction peak was the sum of peaks due to Cu Kα1 and Cu Kα2 lines, it was necessary to separate these two peaks prior to peak broadening evaluation. The mixed peak resulting from Cu Kα1 and Cu Kα2 lines was separated by using the quasi-Voigt function and the difference of wave length between Cu Kα1 and Cu Kα2 lines [5]. In addition, measured peak broadening contained the broadening due to the optical system arrangement of the apparatus. The latter effect on measured peak broadening was corrected based on the measurement results of the unirradiated UO_2 sample.

Table 1
Characteristics of the samples for X-ray diffractometry.

Sample No.	Density at fabrication (%TD)	Grain size at fabrication (μm)	X-ray diffraction position	Local Burnup at X-ray diffraction position[a] (GWd/t)
1	87	12	Periphery	65
			Mid-radius	62
			Central hole edge	62
2	87	13	Periphery	37
			Mid-radius	37
			Central hole edge	43 ± 6[b]
3	94.7	(NA)	Periphery	51
			Mid-radius	51
			Central hole edge	71 ± 20[b]

(NA): not available.
[a] Evaluated from the results of electron prove micro analysis (EPMA), axial gamma scanning and nuclear calculation.
[b] Evaluated from Nd concentration measured by using EPMA (the value corresponds to the apparent burnup).

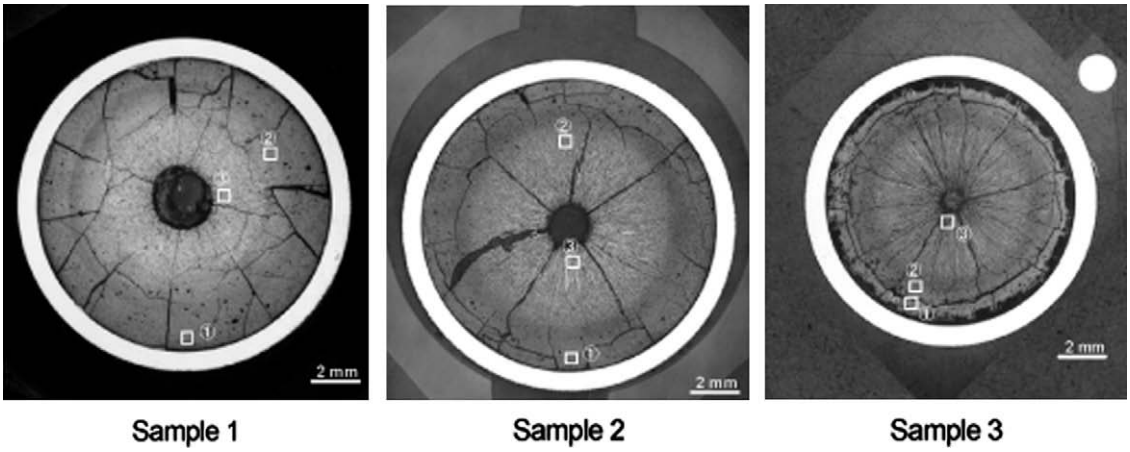

Fig. 2. Macrograph and radial positions of X-ray diffractometry on the cross-sectional surface of each sample. 1: periphery, 2: mid radius, 3: in the vicinity of the central hole.

Non-uniform strain and crystallite size in a sample were evaluated by using the Williamson–Hall method [6]. According to this method, the non-uniform strain and crystallite size in the sample can be expressed as follows:

$$\beta\cos\theta = \frac{k\lambda}{D_x} + 2\eta\sin\theta, \tag{1}$$

where β is the peak broadening corrected for the systematic broadening in 2θ; θ, the diffraction angle; λ, the X-ray wave length; D_x, the crystallite size; and η, the non-uniform strain. The coefficient k is 0.9 when the FWHM of the peak is used as the index of broadening, and the diffraction peak and wave length of Cu Kα1 were used for calculation. The non-uniform strain and crystallite size were obtained by least-squares calculations using twelve diffraction peaks between 45° and 130° in 2θ.

3. Results

3.1. Ceramography and SEM observation results

Fig. 2 shows the macrographs of the etched surfaces of the samples. As seen in the macrographs, macro cracks are observed which formed by the thermal stress due to the radial temperature distribution during irradiation. In addition to the central hole, the columnar grains and pores which elongate along the pellet radial direction are also seen around the central hole in the radial region between the center and mid radius. These pellet microstructure changes indicate that the pellet experienced quite high temperature at the beginning or the end of the irradiation. The dark zone with fine gas bubbles is also observed in the region between the mid radius and periphery of pellet. For sample 1, the region where dense fine bubbles are precipitated and the microstructure at fabrication is unclear was observed at the pellet periphery and also in the dark zone in the pellet: it seems that the rim structure formed in these regions.

Fig. 3 shows the SEM micrographs of the fracture surface on each sample. In these micrographs, the followings are seen: in sample 1, an unevenness which looks like cauliflower is observed on the pore surfaces not only at the periphery but also in the dark zone. This indicates that the rim structure also formed in the dark zone. In the center and mid radius of the pellet, intragranular crack tends to form, and spherical metallic inclusions are seen at grain boundaries and in pores. Grain growth is also seen. In sample 2, since the grain at fabrication is clearly seen, it is considered that a rim structure does not form. Similar to sample 1, intragranular cracks tend to form in the center and mid radius region of pellet, and spherical metallic inclusions are seen at grain boundaries and in pores. Grain growth is also seen. In sample 3, excluding the peripheral region of pellet, the grain at fabrication is seen. This indicates that the rim structure begins to form in the peripheral region. Similar to samples 1 and 2, the intragranular cracks tend to form in the center and mid radius region of pellet, and spherical metallic inclusions are seen at grain boundaries and in pores. Grain growth is also seen.

3.2. Radial burnup profile in the samples

Fig. 4 shows the relative concentrations of Nd and Xe in the radial direction of each sample. The radial profile of Nd corresponds to the radial burnup profile in the sample [4].

The generated Nd profile is almost flat in the relative radius (r/r_0) from 0.5 to 0.8 and gradually increases toward the pellet periphery, and the local relative burnup at the pellet edge becomes approximately 1.2 times of that at mid-radius and center of the pellet. The radial burnup peaking at the periphery of the pellet for the present study is less than that observed in pellets irradiated in light water reactors. This difference is mainly due to the neutron spectrum in the HBWR which is softer than that in a light water reactor, and the self-shielding effect of the fuel pellets is weaker in the HBWR than in light water reactors. On the other hand, the Nd concentration of samples 2 and 3 sharply increases towards the central hole in each pellet. Since the concentration of Nd has an almost flat distribution along the radial direction of pellet in the sample 1 pellet, the effect of the central hole on nuclear properties is negligible. In consideration of the microstructural changes following the irradiation with high linear heat rate near the end of the irradiation experiments, it is considered that the Nd which was accumulated during the irradiation period with low linear heat rate migrated along the radial temperature gradient in the pellet and concentrated in the vicinity of the central hole near the end of the irradiation experiments. As a consequence, the increase of Nd concentration near the central hole of the sample 2 and 3 does not show the real local burnup but the apparent.

Local burnups of X-ray diffraction points were evaluated in consideration of the width of the X-ray radiation area on the specimen surface, and they are summarized in Table 1. The local burnups at the mid-radius and periphery of pellet were nearly the same as the pellet average burnup. The apparent local burnup in the vicinity of the central hole in samples 2 and 3 was estimated from the Nd concentration there as the local burnup is proportional to the Nd concentration.

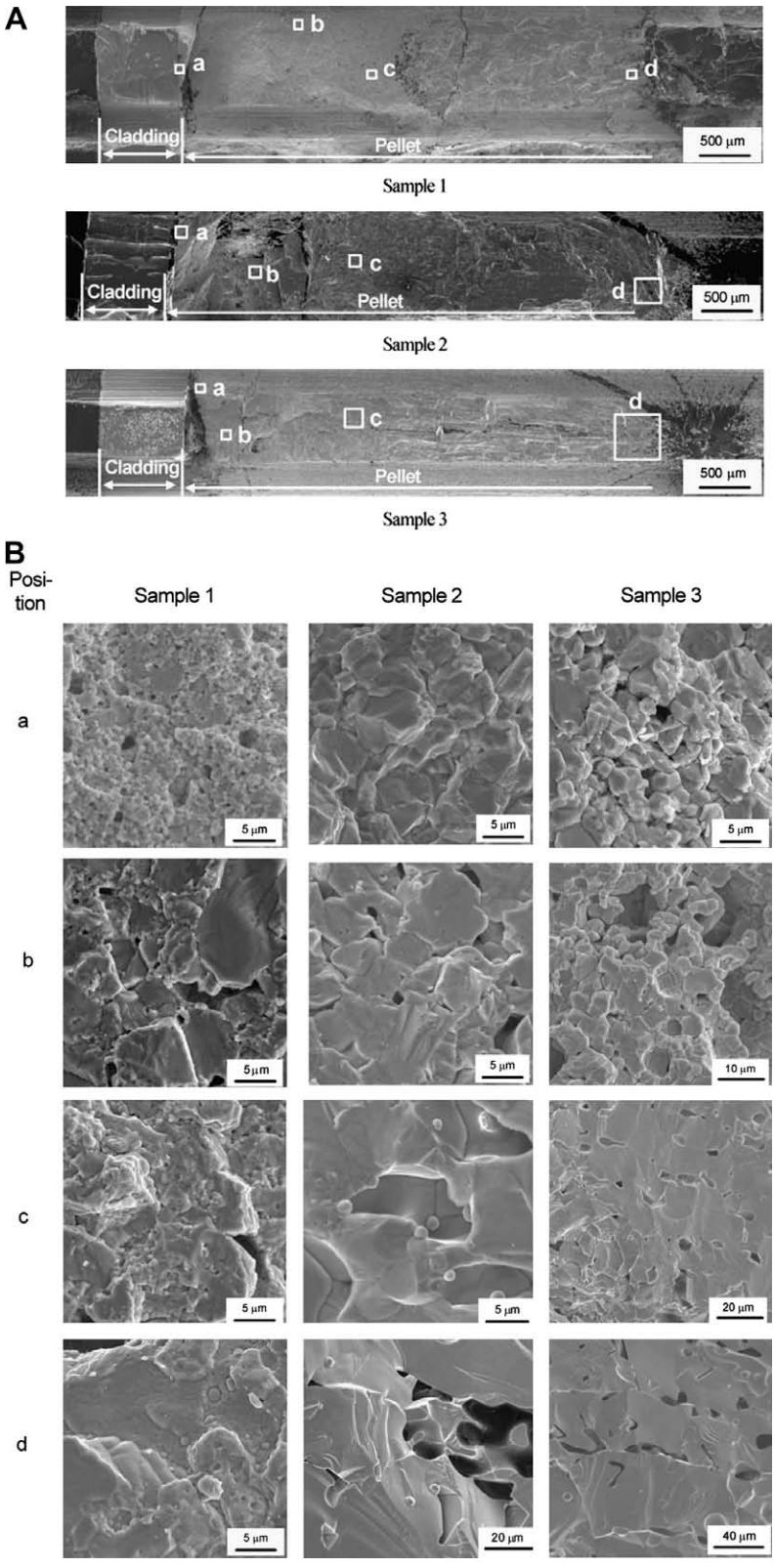

Fig. 3. SEM observation results of fracture surface on each samples. (a) Observation positions of fracture surface on each sample and (b) observation results at each position.

3.3. Lattice parameter change

The burnup dependence of the lattice parameter of irradiated UO_2 samples are shown in Fig. 5. The lattice parameters of irradiated UO_2 reported by several groups [1–4,7,8,16] are also presented for comparison. As seen in the figure, the measured lattice parameters of this study tend to be lower than the reported values. In addition, the lattice parameter near the central hole in each sample shows lower value than that at the mid-radius and periphery of each sample. It is considered that these tendencies are due to

the effect of irradiation temperature and microstructural change during irradiation: this implies that a part of the irradiation-induced defects recovered during the irradiation experiment.

For samples 2 and 3, the lattice parameter in the vicinity of the central hole agrees well with the values estimated from the lattice parameters of soluble FPs-doped UO_2 pellet [9]. This suggests that most irradiation-induced defects recovered, probably following the microstructural change due to the high temperature experienced near the end of the irradiation experiment.

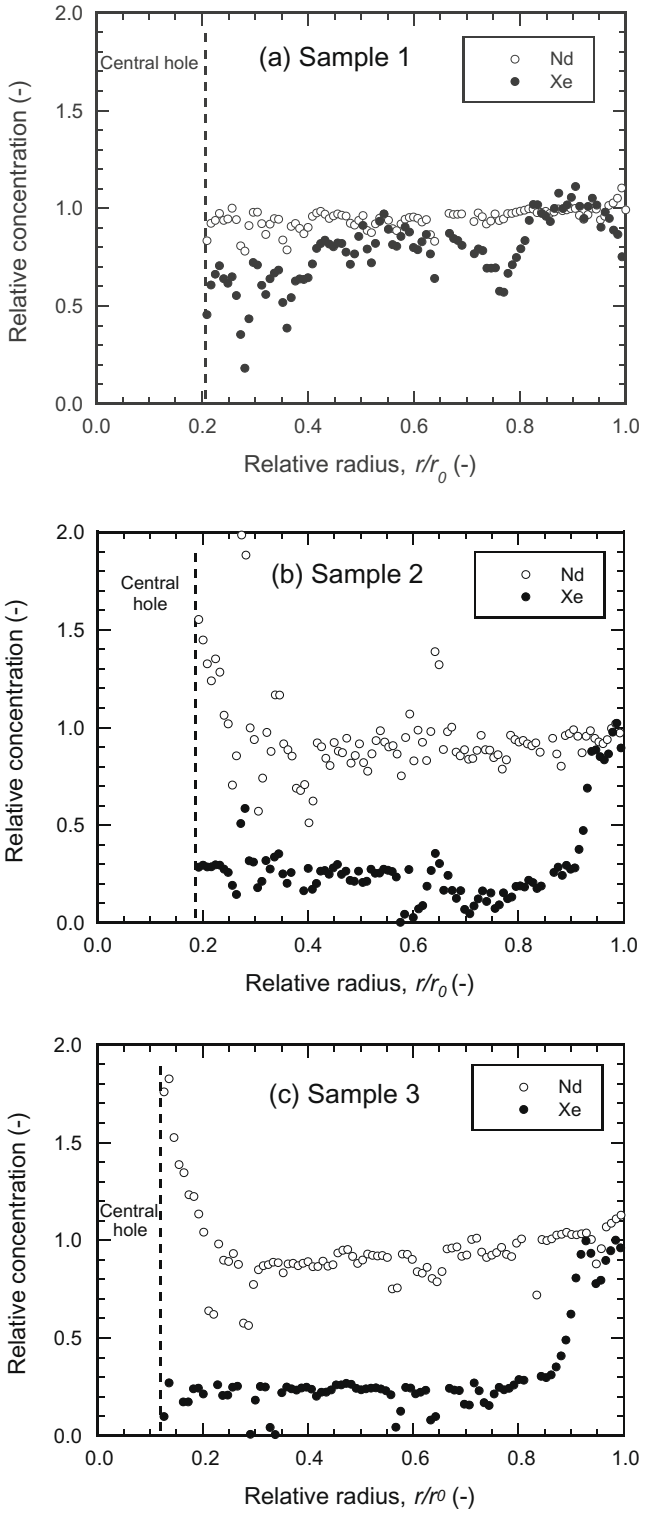

Fig. 4. Radial profiles of the relative concentrations of Nd and Xe in the samples. ○: Nd, ●: Xe.

3.4. Changes in non-uniform strain and crystallite size

The burnup dependences of non-uniform strain and crystallite size in irradiated UO_2 samples are shown in Fig. 6. In the figure, other reported values [4] are also shown for comparison. The non-uniform strain and crystallite size could not be evaluated at the mid-radius and central regions of the sample because the broadenings of diffracted X-ray peaks were hardly observed there.

As seen in the figure, while the non-uniform strains at the periphery of samples 2 and 3 tend to be lower than those in the sample 1 and reported values, the non-uniform strains in sample 1 are in fairly good agreement with the reported values [4]. The crystallite sizes in samples 1–3 are 50–200 nm which is close to the reported values and is similar to that of the subdivided and/or recrystalized grains in the rim structure [10].

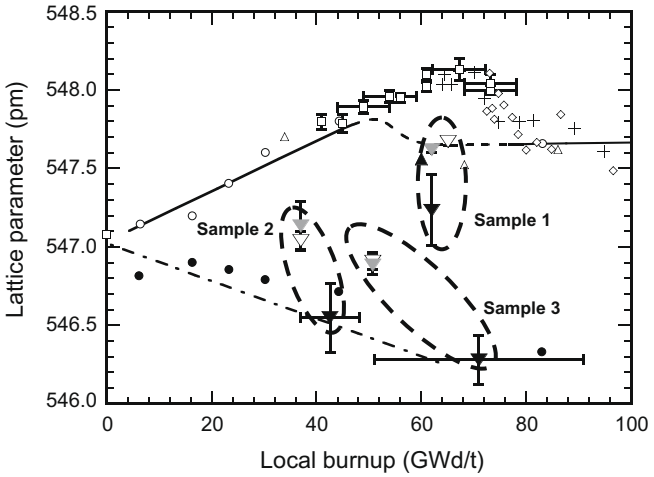

Fig. 5. Local burnup dependence of the lattice parameter of irradiated UO_2 samples. ▽,▼, ▼: this study; ▽: periphery, ▼: mid radius, ▼: in the vicinity of the central hole; ○, ——: Une et al. (irradiated) [1]; ●: Une et al. (annealed) [1]; △: Davies and Ewart [2]; ◇, +: Spino et al. [3]; ▲: Nogita et al. [7]; — · —: Une and Oguma [8]; □: Amaya et al. [4,16].

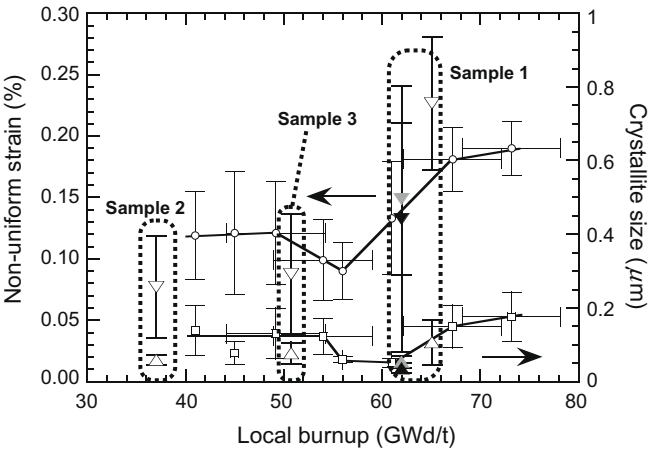

Fig. 6. Local burnup dependence of non-uniform strain and crystallite size in irradiated UO_2 samples. ▽, ▼, ▼: non-uniform strain (this study); ○: non-uniform strain (Amaya et al. [4]); ▽: periphery; ▼: mid radius; ▼: in the vicinity of the central hole; △, ▲, ▲: crystallite size (this study); □: crystallite size (Amaya et al. [4]); △: periphery; ▲: mid radius; ▲: in the vicinity of the central hole.

3.5. Strain energy density in irradiated UO_2 sample

The strain energy density which is accumulated in irradiated UO_2 samples can be expressed as the sum of the strain energy densities due to crystal lattice strain and the non-uniform strain occurring between crystallites. The total strain in an irradiated sample can be divided into crystal lattice strain (ε_c) and non-uniform strain (ε_{nu}):

$$\varepsilon_{\text{tot}} = \varepsilon_c + \sqrt{\frac{2}{\pi}}\varepsilon_{nu}. \tag{2}$$

The crystal lattice strain ε_c is evaluated from the lattice parameter changes between irradiated and simulated soluble FPs-doped UO_2 as follows:

$$\varepsilon_c = \left(\frac{a - a_{\text{FP}}}{a_{\text{FP}}}\right), \tag{3}$$

where a is the lattice parameter of the irradiated sample; and a_{FP}, the lattice parameter of soluble FPs-doped UO_2 with simulated burnup of irradiated sample [8].

It is considered that the strain occurring in an irradiated UO_2 sample is isotropic because the lattice structure of the UO_2 is fluorite and preferred orientation was not clearly observed in non-uniform strain. Accordingly, the strain energy density, U, can be evaluated as follows:

$$U = \frac{3}{2}E\varepsilon_{\text{tot}}^2, \tag{4}$$

where E is the Young modulus.

Fig. 7 shows the burnup dependence of strain energy density of irradiated UO_2 samples. In the figure, other reported values [4] are also shown for comparison. As seen in the figure, the strain energy density tends to increase with burnup and levels off at burnups of approximately 50 and 70 GWd/t. The strain energy density in the peripheral region of sample 1 agrees well with the trend of the reported values. The strain energy densities in the central and mid radius region of sample 1 tend to be lower than that in the peripheral region. The strain energy densities in the peripheral regions of samples 2 and 3 are lower than those of sample 1. It is likely that the decrease of strain energy density in the peripheral regions of samples 2 and 3 is related to the effect of high temperature: samples 2 and 3 were irradiated under high linear heat rate conditions just before the end of the irradiation tests.

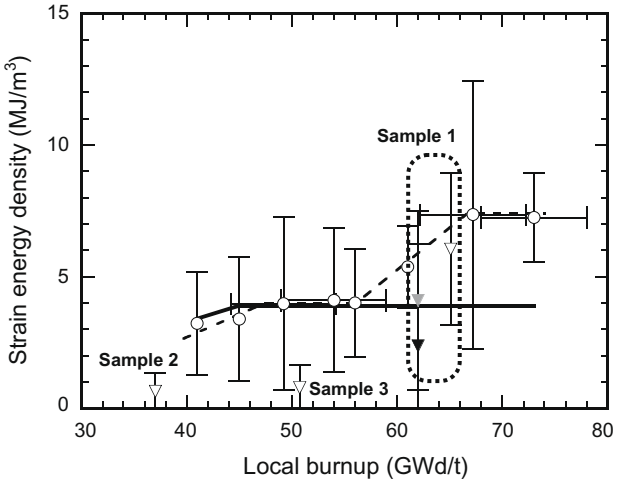

Fig. 7. Local burnup dependence of strain energy density of irradiated UO_2 samples. ▽, ▼, ▼: this study; ▽: periphery; ▼: mid radius; ▼: in the vicinity of the central hole; ○: Amaya et al. [4]; - - - -: the trend of the measured values [10]; ——: the value calculated from the dislocation densities [10].

4. Discussion

4.1. Effect of alpha-damage on the lattice parameter of irradiated UO_2 pellet

Since it was reported that the lattice parameter of UO_2 single crystal increased after being irradiated with alpha particle due to the effect of "alpha-damage" [11], it is necessary to investigate the effect of alpha-damage on the lattice parameter of irradiated UO_2 pellets because some amount of plutonium is accumulated in the pellets during irradiation.

In the case of the irradiation experiment using the HBWR, since heavy water is used as coolant, the neutron spectrum in the reactor is quite soft compared with that in light water reactors. Due to this nuclear characteristic of the HBWR, it is considered that the amount of the plutonium accumulated during irradiation in the HBWR is quite small and the effect of alpha-damage on the lattice parameter of pellets irradiated in the HBWR is not significant compared to those of the pellets irradiated in light water reactors. In addition, it is considered that the effect of (O/M) ratio on the lattice parameter is negligible in these samples because the (O/M) ratio of irradiated UO_2 pellets is very close to 2 from the view point of the oxygen potential of irradiated UO_2 up to 200 GWd/t [12].

In consideration of the power histories of samples 2 and 3, it is not appropriate to compare the lattice parameters of these samples directly with the values of the samples irradiated in light water reactors. On the other hand, since the power history of sample 1 is relatively close to the typical power history of fuel rods in light water reactors excluding the power history at the beginning of irradiation test, the lattice parameter of sample 1 may be compared with the values of samples irradiated in light water reactors.

As seen in Fig. 5, the lattice parameters at the mid-radius and periphery of sample 1 are relatively close to those of samples irradiated in light water reactors. Considering that microstructural changes which were similar to rim structure formation were observed at both positions in sample 1 and the values agree well with the values in the burnup region above 80 GWd/t where the rim structure forms, the lattice parameter difference between sample 1 and the samples irradiated in light water reactors may be due to the microstructural change. Consequently, it is likely that the effect of alpha-damage is not dominant to the lattice parameter change in the samples of this study and also in UO_2 samples irradiated in light water reactors.

4.2. Effect of accumulated dislocation on the strain energy density in irradiated UO_2 samples

According to the results of TEM (transmission electron microscopy) observations by Nogita et al. [13], dislocation densities in irradiated UO_2 increased in the range up to 44 GWd/t and saturated due to dislocation tangles, and it may be appropriate to consider that the formed dislocation is mainly an edge dislocation from its appearance and behavior [4,13].

Elastic strain energy density of edge dislocation per unit length, U_{dis}, is expressed as follows:

$$U_{\text{dis}} = U_{\text{dis1}} + U_{\text{dis2}}, \tag{5}$$

where U_{dis1} and U_{dis2} are the elastic strain energy densities in the outside and inside of the edge dislocation core, respectively. The terms of U_{dis1} and U_{dis2} can be expressed as [14]:

$$U_{\mathrm{dis1}} = \frac{\mu b^2}{4\pi(1-\nu)} \ln\frac{r_1}{r_0}, \tag{6}$$

$$U_{\mathrm{dis2}} = \frac{\mu b^2}{8\pi(1-\nu)^2}, \tag{7}$$

where μ is the shear modulus; b, the Burgers vector; ν, the Poisson ratio; r_1, the radius of stress region affected by dislocations; and r_0, the radius of the edge dislocation core.

Elastic strain density of dislocation per unit volume, U_{disV}, can be expressed as:

$$U_{\mathrm{disV}} = \rho \cdot U_{\mathrm{dis}}, \tag{8}$$

where ρ is the dislocation density per unit volume.

For irradiated UO_2, the strain energy densities induced due to the accumulation of dislocations were calculated using the data shown in Table 2. Fig. 7 compares the values calculated using Eqs. (5)–(8) with the measured values. As seen in the figure, the calculated strain energy density in the central region of sample 1 tends to be higher than the values shown as the solid line. This implies that other accumulation mechanisms of strain energy density exist in addition to the accumulation of dislocations, such as crystallite rotation [4]. The calculated strain energy density in the mid radius region of sample 1 is in fairly good agreement with the values shown as the solid line. This indicates that the main source of strain energy is the accumulation of dislocations in the mid radius region of sample 1.

4.3. Burnup dependence of the strain energy density in irradiated UO_2 samples

As seen in Fig. 7, it seems that the burnup dependence of strain energy density in irradiated UO_2 sample tends to change at about 55 GWd/t. In the region below a burnup threshold of about 55 GWd/t, the lattice parameters of irradiated UO_2, that is the uniform strains, increase monotonously, while the non-uniform strains hardly change or slightly decrease. On the other hand, in the region above the threshold, the non-uniform strains increase while the lattice parameters level off and tend to decrease. In consideration of the amount of the crystal lattice strain formed by point defects in UO_2 [17,18], these tendencies suggest the following things: interstitial atoms which cause uniform strain begin to form dislocations as a recovery process of irradiation defects and the dislocation density increases in the former region, while the accumulation of dislocations in the crystallite saturates and the migration of dislocations becomes dominant as a recovery process of irradiation defects in the latter region. In other words, it is considered that a part of the point defects accumulated in the crystallite such as vacancies is swept out to the outside of crystallite in the latter region following the migration of dislocations. The sweep-out of vacancies causes a volume change in the crystallite and may cause additional strain distribution among crystallites. Following this, an additional increase in strain energy density may be generated in the latter region. The vacancies which are swept out from the crystallites by the migration of dislocations may be a source of the coarsened bubble formation in the rim structure.

5. Conclusions

Pellet samples were prepared from three kinds of fuel rods which were irradiated in the Halden Heavy Water Reactor (HBWR) in Norway, and microstructural changes in the pellet samples were investigated by means of optical microscopy, scanning electron microscopy/electron probe micro analysis (SEM/EPMA) and micro-X-ray diffractometry. Pellet-averaged burnups were in the range of 37–62 GWd/t. Based on the micro-X-ray diffraction results, lattice parameters and diffraction peak broadenings (increase of FWHM of diffraction peak) of the samples were measured. Crystallite size and non-uniform strain between crystallites were evaluated from the increases of FWHM of the diffraction peaks using the Williamson–Hall method.

The measured lattice parameters tended to be smaller than the values reported previously. Since the samples 2 and 3 experienced high temperature near the end of the irradiation test, it is likely that the lattice parameters of samples 2 and 3 decreased owing to the recovery of irradiation-induced defects. The lattice parameter decreases at the periphery and mid radius of sample 1 are probably affected by the microstructural changes, because a microstructure which is quite similar to the rim structure was observed there and the measured lattice parameters are comparable with the values reported in the high burnup region where the rim structure forms. Considering the difference in neutron spectrum between the HBWR and typical light water reactors, this tendency suggests that the effect of alpha-damage on lattice parameters is not significant in high burnup UO_2 pellets.

Measured crystallite sizes of irradiated samples were in the range of 50–200 nm and these were nearly the same size as the sub-divided and/or recrystalized grains in the rim structure. Elastic strain energy densities in the samples were also evaluated based on the crystal lattice and non-uniform strain. In the region below a burnup threshold of about 55 GWd/t, the lattice parameters of irradiated UO_2, that is the uniform strains, increase monotonously, while the non-uniform strains hardly change or slightly decrease. On the other hand, in the region above the threshold, the non-uniform strains increase while the lattice parameters level off and tend to decrease. These tendencies suggest the following things: the interstitial atoms which generate uniform strain begin to form dislocation as a recovery process of irradiation defects and the dislocation density increases in the former region, while the accumulation of dislocations in the crystallite saturates and the migration of dislocations becomes dominant as a recovery process of irradiation defects in the latter region. Due to the migration of dislocations, a part of the point defects in the crystallite such as vacancies is swept out to the outside of the crystallite. The sweep-out of vacancies causes volume changes in the crystallite and may cause additional strain distribution among crystallites. Following this, the additional increase in strain energy density may be generated in the latter region. The vacancies which are swept out from the crystallites by the migration of dislocations may be a source of the coarsened bubble formation in the rim structure.

Table 2
Data used in calculation of strain energy density due to accumulation of dislocation.

Shear modulus μ [15]	77 GPa
Burgers vector b [10]	0.39 nm
Poisson ratio ν [15]	0.31
Dislocation density ρ [12]	$\log \rho = 2.2 \times 10^{-2}$ Bu + 13.8 ($6 \leqslant$ Bu $\leqslant$ 44 GWd/t) = 14.77 (Bu > 44 GWd/t) ρ in m/m^3 and Bu in GWd/t)
Radius of stress region affected by dislocation r_1	$1/\sqrt{\rho}$
Radius of dislocation core r_0	0.55 nm (derived from the lattice parameter of UO_2 [13,16])

Acknowledgments

The authors are grateful to the OECD Halden Reactor Project (HRP) for supplying irradiated fuel rods for the tests. They would like to thank their colleagues in the Fuel Safety Research Group and in the Reactor Fuel Examination Facility for their excellent post-irradiation examinations.

This study was financially supported by the Budget for Nuclear Research of the Ministry of Education, Culture, Sports, Science and Technology, based on the screening and counseling by the Atomic Energy Commission.

References

[1] K. Une, K. Nogita, S. Kashibe, et al., J. Nucl. Mater. 188 (1992) 65.
[2] J.H. Davies, F.T. Ewart, J. Nucl. Mater. 41 (1971) 143.
[3] J. Spino, D. Papaioannou, J. Nucl. Mater. 281 (2000) 146.
[4] M. Amaya, J. Nakamura, T. Fuketa, J. Nucl. Sci. Technol. 44 (2008) 255.
[5] T. Takahashi, Imono 65 (1993) 13 (in Japanese).
[6] G.K. Williamson, W.H. Hall, Acta Metal. 1 (1953) 22.
[7] K. Nogita, K. Une, M. Hirai, et al., J. Nucl. Mater. 248 (1997) 196.
[8] K. Une, M. Oguma, J. Nucl. Sci. Technol. 20 (1983) 844.
[9] K. Nogita, K. Une, J. Nucl. Sci. Technol. 30 (1993) 900.
[10] K. Nogita, K. Une, J. Nucl. Mater. 226 (1995) 302.
[11] W.J. Weber, J. Nucl. Mater. 98 (1981) 206.
[12] Hj. Matzke, J. Nucl. Mater. 223 (1995) 1.
[13] K. Nogita, K. Une, Nucl. Inst. Meth. Phys. Res. B 91 (1994) 301.
[14] T. Yokobori et al., Kinzokuzairyou-No-Kyoudo-To-Hakai, Nippon-Kinzoku-Gakkai-Kyoudo-Iinkai, Maruzen, Tokyo 100 (1964) (in Japanese).
[15] A. Padel, Ch. de Novion, J. Nucl. Mater. 33 (1969) 40.
[16] M. Amaya, K. Une, M. Hirai, J. Nucl. Sci. Technol. 41 (2004) 108.
[17] M. Iwasawa, T. Onuma, Y. Kaneta, et al., in: Proc. 2007 Fall Annual Mtg Japan Institute of Metals, Gifu, Japan, September 19–21, 120, The Japan Institute of Metals, 2007 (in Japanese).
[18] M. Iwasawa, T. Onuma, Y. Kaneta, et al., in: Proc. 2006 Fall Annual Mtg Japan Institute of Metals, Niigata, Japan, September 16–18, 924, The Japan Institute of Metals, 2006 (in Japanese).